Nonlinear Analytical Model-Embedded Optimal Design for ER-PMSM

Ang Liu[1], Xiaoyan Huang[1], Zhuo Chen[1], Ye Ma[1], Yelong Yu[1], Zhaokai Li[2]

[1]College of Electrical Engineering, Zhejiang University, Hangzhou, 310027, China
[2]School of Electrical Engineering and Computer Science, KTH Royal Institute of Technology, Stockholm 11428, Sweden

This paper proposed a nonlinear analytical model-embedded optimal design procedure for permanent-magnet synchronous motors with an external rotor. Combined with the winding inductance calculation, a refined magnetic circuit is proposed for the analytical prediction of the electromagnetic performance. The stator nonlinearity, which is significant in torque prediction, is considered by using the conception of saturation current. Then, ant colony algorithm is employed for the multi-objective optimization for the great potential in global exploring. Finally, optimal design parameters are selected from the Pareto front. The effectiveness of the proposed optimization design method is verified by finite-element analysis and experimental results of the manufactured prototype.

Index Terms—external rotor PMSM, winding function, magnetic equivalent circuit, multi-objective optimization.

I. Introduction

The external rotor permanent-magnet synchronous motor (ER-PMSM) is widely used in drones and robotics for its impressive torque performance. Optimal design with single objective of ER-PMSM can be analytically achieved by linear model [1], which is well matched with finite-element analysis (FEA) results at low load conditions. For multi-objective case, an ant colony optimization is used to generate Pareto front based on linear analytical formulas [2]. However, the linear model loses accuracy when the motor is operated with large winding current, leading to heavy iron saturation [3]. Thus, it is common to use FEA as a general approach for optimal design in ER-PMSMs [4]. Different optimization algorithms based on FEA are adopted in multi-objective design to generate pareto fronts [5], [6], which suffer from long calculation time. To reduce the computational burden, analytical models including conformal mapping and subdomain, together with magnetic equivalent circuit are used to calculate the electromagnetic performance for single case [7], [8] It is noted that the stator saturation effect is well considered in these literatures, which has a significant impact on the output torque.

This paper proposed a nonlinear analytical model (NAM) which involves the stator saturation. The air-gap field at no load condition is analytically predicted, and the armature reaction field is established by the winding function. The equivalent magnetic circuit in stator core is then iteratively solved according to the given B-H curve. Based on the proposed NAM, an ant colony algorithm is used for the multi-objective optimization. The whole calculation procedure can be finished with high calculation speed and accuracy. The final design is validated with FEA results and the experimental results.

II. Nonlinear Analytical Model

The assumptions are made as follows for the proposed model: 1) the rotor iron has infinite permeability [9], [10]; 2) the property of PM is linear; 3) the edge effect is neglected. The symbol of the parameterized motor geometry is shown in Fig. 1 (a).

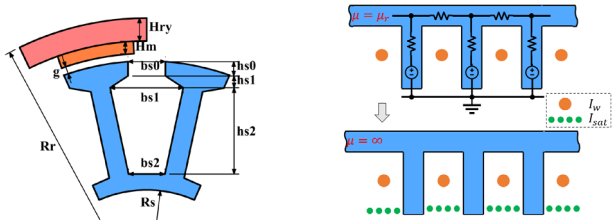

(a) Geometry parameterization (b) Magnetic equivalent circuit in stator

Fig. 1 The 36-slot/42-pole model of ER-PMSM.

A. Air-gap Field at No Load Condition

According to [9], the flux density B_g by permanent magnet at the stator surface is given by the scalar potential

$$B_g = -\mu_0 \vec{\nabla} \sum_k \left(A_k r^{-k} + B_k r^k \right) \cos k\theta \tag{1}$$

where μ_0 is the permeability in vacuum; A_k and B_k are constants; k represents the harmonic order of Fourier series and θ is the rotor position. Hence, the flux linkage in stator coil is represented as the integral of B_g [7]:

$$\varphi_{PM,t} = N_t l_{ef} R_g \int_{\theta_t - \alpha_P/2}^{\theta_t + \alpha_P/2} B_g d\theta \tag{2}$$

where N_t, l_{ef} and R_g are the turns of coil, stack length, air-gap radius, and the number of slots, respectively. θ_t is the central position of coil t, and α_P is the slot-pitch angle.

B. Winding Inductance Calculation

At load condition, the magnetic motive force (MMF) given by stator coil with phase current i is [11]:

$$F(x) = \sum_{v=1}^{\infty} \frac{2iN_t}{v\pi} \sin\left(v\frac{\theta_y}{2} \right) \frac{\sin\left(v\theta_s/2 \right)}{v\theta_s/2} \cos(vx) \tag{3}$$

where x is the distance to the central point of the slot; θ_y is the short pitch angle; v represents the harmonic orders; θ_s is the angle of slot opening in mechanical radians.

Therefore, the magnetizing inductance is calculated as

$$l_m = \frac{\varphi_{coil}}{i} = N_t l_{ef} R_g \int_{-\pi/Z}^{\pi/Z} \frac{1}{i} \lambda_g F(x) dx \tag{4}$$

where φ_{coil} is the magnetizing flux in the coil, Z is the number of stator slots and λ_g is the airgap permeance [12]. As for leakage inductance, the slot leakage inductance l_{tt} and tooth top leakage inductance l_{ss} can be given according to the slot geometry [11]:

$$l_{tt} = \mu_0 N_t^2 l_{ef} \frac{5g_e}{5b_{s0} + 4g_e} \tag{5}$$

$$l_{ss} = \mu_0 N_t^2 l_{ef} \left(\frac{h_{s0}}{b_{s0}} + \frac{2h_{s1}}{b_{s0} + b_{s1}} + \frac{2h_{s2}}{3\left(b_{s1} + b_{s2}\right)} \right) \tag{6}$$

where g_e is the equivalent airgap length, b_{s0}, b_{s1} and b_{s2} are the widths of slot opening, slot top and slot bottom, respectively, and h_{s0}, h_{s1} and h_{s2} are for the heights. The inductance matrix $\mathbf{L_s}$ is then generated, which gives the linear relationship between coil current and the corresponding flux linkage.

C. Magnetic Equivalent Circuit

The magnetic equivalent circuit of inner stator is shown in Fig. 1 (b), based on the concept of flux tube [8]. According to Kirchhoff's law, the field distribution can be solved by

$$f\left(\mathbf{V}\right) = \mathbf{G_m V} - \mathbf{\Phi}_s = 0 \tag{7}$$

where $\mathbf{V}$ is the node magnetic potential vector of the stator. $\mathbf{G_m}$ is the branch permeance matrix, consisting of stator teeth and yoke permeance. $\mathbf{\Phi_s}$ is the flux vector of stator teeth.

The saturation current is introduced to take the iron non-linearity into account. According to Ampere's law, the saturation current in the loop of a slot should be equal to the magnetic potential drop on stator teeth and yoke. Thus, the flux flowing into the stator core can be expressed as the sum of the flux produced by PMs and the winding current, so as the saturation current.

$$\mathbf{\Phi_s} = \mathbf{\Phi_{PM}} + \mathbf{L_S}\left(\mathbf{I_s} - \mathbf{I_{sat}}\right) \tag{8}$$

where $\mathbf{\Phi_{PM}}$ is the flux linkage produced by permanent magnets, $\mathbf{I_s}$ and $\mathbf{I_{sat}}$ are the vectors of winding current and saturation current, respectively. The general solution of the proposed NAM is then derived from the calculation of magnetic equivalent circuit shown in Fig. 1, after substituting (8) into (7), we have

$$\mathbf{G_m V} - \mathbf{\Phi_{PM}} - \mathbf{L_S}\left(\mathbf{I_s} - \mathbf{I_{sat}}\right) = 0 \tag{9}$$

where the nonlinear permeances in $\mathbf{G_m}$ are calculated according to the B-H curve of stator shown in Fig. 5. The Newton-Raphson method is used to find the solution in iteration cycles, in which the iteration of saturation current is given by

$$\mathbf{I_{sat,n+1}} = \left(1 - \alpha_r\right)\mathbf{I_{sat,n}} + \alpha_r \mathbf{L_S^{-1}}\left(\mathbf{\Phi_{PM}} + \mathbf{L_S I_s} - \mathbf{G_m V}\right) \tag{10}$$

where α_r is the relaxation factor to accelerate the convergence of iterative calculation.

D. Calculation of Torque

After iterative calculation for the back electromagnetic force (EMF) in each coil, the electromagnetic torque can be expressed as [13]:

$$T = \frac{P_{em}}{\Omega} = \frac{\sum_{i=1}^{Z} e_i i_i}{\Omega} = \frac{\sum_{i=1}^{Z} \left(-d\varphi_i / dt\right) i_i}{\Omega} \tag{11}$$

where Ω is the mechanical speed.

III. MOAC-based Optimization Algorithm

The multi-objective ant colony (MOAC) optimization is employed in this paper based on the electromagnetic performance calculation by NAM. The current density condition is introduced as the thermal limitation in this paper, since it is concluded in [14] that it is a severer limitation for the small size machine with high load requirement. More specifically, the current density is firstly defined as J = 20 A/mm^2 and kept the same during the subsequent optimization. Besides, constraint function of $b_{s2} > 0$ is evaluated to avoid the potential geometric interference.

The parameter sensitivity of different design variables are calculated by equation (12) [15] and the bar chart of multi-objective sensitivity analysis is given in Fig. 2.

$$S\left(x\right) = E\left(S\left(x_i\right)\right) = E\left(\frac{f\left(x_0 + \Delta x_i\right)/f\left(x_0\right) - 1}{\Delta x_i / x_0}\right) \tag{12}$$

where x_i is the design variable of ER-PMSM and x_0 is the value of initial case. $f(x)$ represents the objective function which can be expressed as $\{T/m \;\; V_{magnet}\}$. m and V_{magnet} represent the weight of the prototype and the volume of magnet, respectively, which can be derived with the knowledge of motor dimensions.

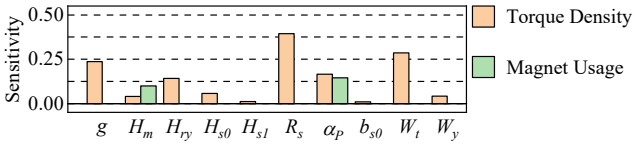

Fig. 2 Sensitivity analysis results of different design variables.

Fig. 2 shows that the structure dimension of stator tooth tip has negligible influence on the output torque and the usage of magnets. Then, the input design variables are reduced and the variable ranges are listed in TABLE. I.

TABLE. I
Initial Value and Ranges of Design Variables

Parameter	Definition	Initial value	Range
g (mm)	Airgap length	0.8	0.5-1
H_{ry} (mm)	Height of rotor yoke	2.5	2-3.5
α_P	Pole arc coefficient	0.75	0.55-0.85
D_s(mm)	Stator bore	64	40-70
H_m (mm)	Magnet thickness	2	1-3
W_t (mm)	Width of stator teeth	3	2-4

Unlike the commonly used weighting average function [16], [17] which scalarize the multi-objective optimization to a single-objective problem, the objective targets are manipulated individually to generate the Pareto front. The selection probability of each discrete value of design variables can be calculated by

$$p_{ij} = \tau_{ij}^{\alpha} \eta_{ij}^{\beta} \Big/ \Sigma_{j=1}^{m} \tau_{ij}^{\alpha} \eta_{ij}^{\beta} \tag{13}$$

where τ is the pheromone concentration and η is the heuristic factor to increase trial case diversity and avoid local convergence. The index α, β is chosen between [0,1] to get a balance between the speed of convergence and global searching capability. τ is given by the summation of pheromone volatilized by each non-dominate solution, which is represented by its average distance to other Pareto results

$$\tau_{ij}\left(\xi\right) = \tau_{ij}\left(\xi - 1\right) + \sum_{m}\sum_{n}\left[f_n\left(k\right) - f_n\left(m\right)\right]^2 \tag{14}$$

where f_n represent the different optimization functions. In this paper, they are torque density and volume of permanent magnet. Finally, the optimization procedure is given in Fig. 3 .

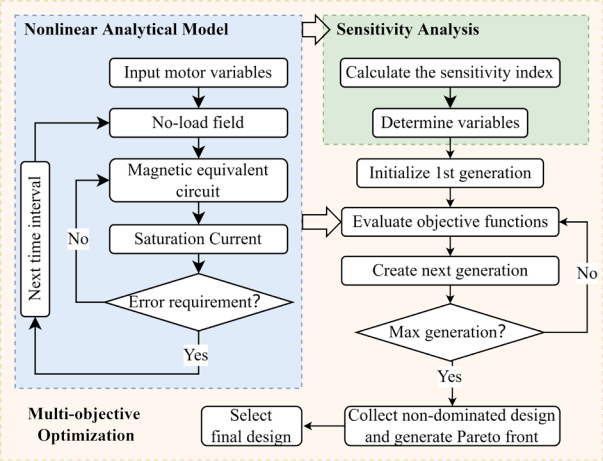

Fig. 3 Flow chart of the proposed nonlinear analytical model based optimal design procedure.

IV. FE Simulation and Experimental Verification

In order to guarantee the accuracy of the proposed method, the electromagnetic performance of many cases on the Pareto front in the multi-objective design need to be verified. However, experimental validation is only suitable for a single prototype with specificized design parameters. It is obviously rather difficult to verify all the designs by experiments. To solve this problem, the FE model of a 36-slot/42-pole motor is introduced using JMAG software package, as shown in Fig. 4. Existing literatures prove that the calculation results of FEA always agree well with the experimental validation. Similarly, the generated Pareto fronts of FEA and the proposed NAM are compared in this section, to verify the effectiveness of this multi-objective design procedure. Also, the limitation of linear model is demonstrated, since the iron nonlinearity becomes severe in stator core, especially in the stator teeth at rated load condition, the iron nonlinearity becomes severe in stator core, especially in the stator teeth.

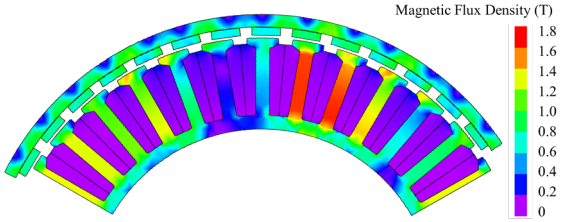

Fig. 4 The 36-slot/42-pole model of ER-PMSM in FEA.

Besides, the electrical steel 20JNEH1200 is used for stator and the stainless steel SCM420 is employed for the rotor to guarantee structural strength in such small height of rotor yoke. The electrical characteristics of the materials are specificized in TABLE. II. Their B-H curves are shown in Fig. 5.

TABLE. II
Electrical Characteristics of the Materials

	Resistivity (Ω·m)	Magnetic Flux Density (T) @H=1000 A/m	@H=5000 A/m	@H=10000 A/m	Density (g/cm^3)
20JNEH1200	5.5e-7	1.49	1.69	1.79	7.65
SCM420	2.54e-7	0.58	1.52	1.73	7.79

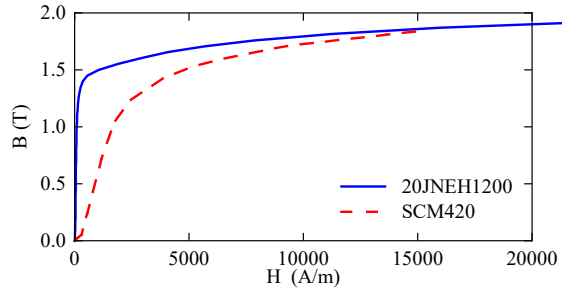

Fig. 5 The B-H curves of magnetic materials for ER-PMSM.

The Pareto fronts generated by NAM and FEM are compared in Fig. 6. Selected from the Pareto front, the main parameters of the final design are listed in TABLE. III. The electromagnetic performance of the prototype is measured at the test rig to validate the proposed model, as shown in Fig. 7.

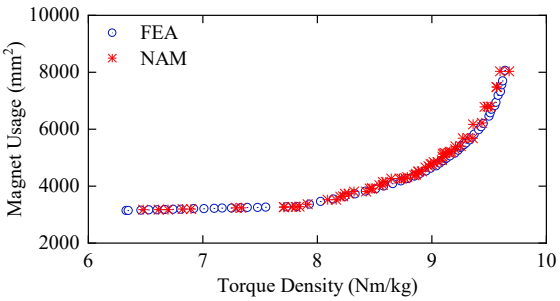

Fig. 6 Comparisons of Pareto fronts between NAM and FEM.

TABLE. III
Dimensions of 36-Slot/42-Pole PMSM

	Parameter	Value	Parameter	Value
Stator	Outer Diameter	92.2mm	Effective Length	20mm
	Inner Diameter	60mm	Tooth width	2.4mm
	Material	20JNEH1200	Yoke width	2.4mm
Rotor	Outer Diameter	100mm	Material	SCM 420
	Inner Diameter	92.8mm		
Magnet	Material	N38H	Thickness	1.4mm

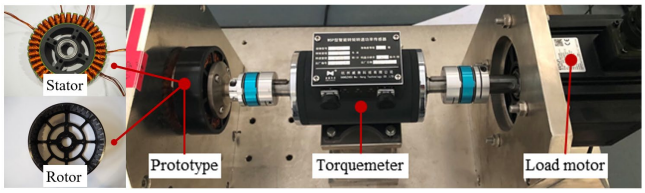

Fig. 7 The manufactured prototype and experimental rig.

A. Flux Linkage and Back-EMF

Fig. 8 illustrates that the flux linkage prediction by NAM in stator winding is accurate compared with FEA results. The errors caused by the linear analytical model (LAM) grow larger with the increase of winding current due to neglecting iron saturation, but NAM predictions still agree well with FEA results.

The waveform of back-EMF is calculated by the derivative of flux linkage. As shown in Fig. 9, LAM tends to overestimate the amplitude of back-EMF compared with the tested result while NAM agrees well with measured back-EMF.

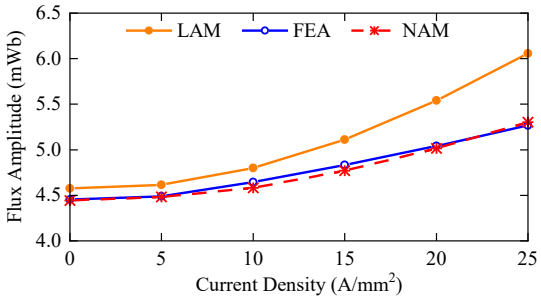

Fig. 8 Variation of flux linkage amplitude to current density.

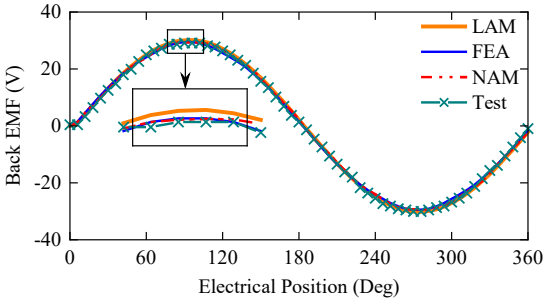

Fig. 9 The measured and calculated back EMF waveforms.

B. Electromagnetic Torque

The proposed nonlinear model gives accurate results of electromagnetic torque in Fig. 10. As for linear model, the error can be greater than 6%. It should be noted that this model only focuses on the computation of average value and the torque ripple is not the main concern. To validate the effectiveness of the proposed model at different load conditions, the electromagnetic torque is calculated at different current amplitude in Fig. 11. With the current growing up, the saturation in stator iron gradually increases. NAM agrees well with FEA, while linear model overestimates the torque with an increasing error. Test results agree well with FEM at low current density, while the largest error occurs at the heaviest load condition for the risen temperature of rotor magnets.

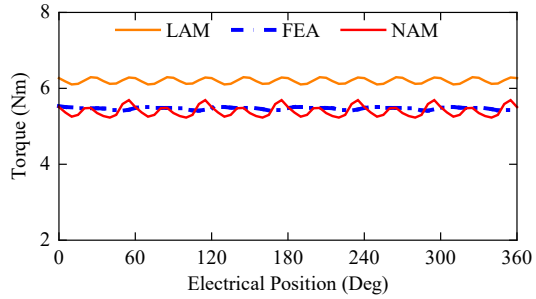

Fig. 10 The comparison of torque waveforms at J=20A/mm^2.

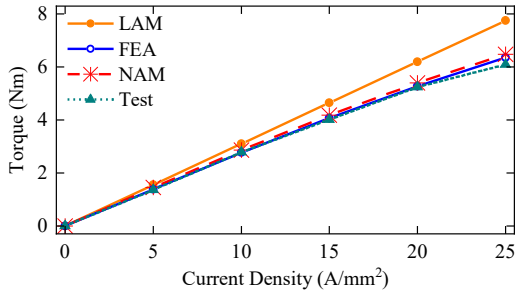

Fig. 11 The comparison of average torque at different load conditions

C. Calculation Time

The proposed method is time sparing even compared with other hybrid model, for the simplified structure of magnetic circuit. The main time-consuming part is the solving process of saturation current and it could be solved in few seconds. The calculation time of NAM and FEM for computing average torque is given in TABLE. IV. Obviously, it saved more than 99% of the calculation time using FEA both in the single case calculation and the multi-objective optimization.

TABLE. IV
COMPARISON OF COMPUTATION TIME

Computation Time	NAM	FEA	Difference Percentage
No Load [s]	0.29	114	
Rated Load [s]	0.34	120	↓99%
Multi-objective Optimization [min]	8.75	2910	

V. CONCLUSIONS

This paper proposed a NAM focusing on the torque reduction due to stator iron saturation and it significantly reduces the computational burden. Based on the winding inductance prediction, the magnetic equivalent circuit is simplified to accelerate the solving process. With the help of equivalent saturation current, the proposed model accurately predicted the average torque of ER-PMSM with different geometry parameters at various load conditions. Then a MOAC model is developed to determine the Pareto front in search space, from which the final design is selected. Finally, a prototype is manufactured to verify the effectiveness of proposed model. The proposed method will become a time saving tool for the analysis and optimization of ER-PMSM. For more detailed analysis such as cogging torque and efficiency performance, further analysis based on FEA can be used for the validation of the final design.

Compared with fixed current density, thermal models will give a more accurate thermal restriction in the motor design procedure, which will be our future work. Due to the increased computational burden, the fuzzification technique-based data preprocessors will be conductive to accelerate the calculate process and decrease the overall system noise [18], [19].

ACKNOWLEDGMENT

This work was supported by the National Key R&D Program of China (2019YFE0123500) and Natural Science Foundation of China under grant 51837010.

REFERENCES

[1] Y. Shen and Z. Q. Zhu, "Analytical Prediction of Optimal Split Ratio for Fractional-Slot External Rotor PM Brushless Machines," *IEEE Trans. Magn.*, vol. 47, no. 10, pp. 4187–4190, Oct. 2011, doi: 10.1109/TMAG.2011.2147286.

[2] Y. Li, C. Zhu, L. Wu, and Y. Zheng, "Multi-Objective Optimal Design of High-Speed Surface-Mounted Permanent Magnet Synchronous Motor for Magnetically Levitated Flywheel Energy Storage System," *IEEE Trans. Magn.*, vol. 55, no. 7, pp. 1–8, Jul. 2019, doi: 10.1109/TMAG.2019.2906994.

[3] Đ. Lekić and S. Vukosavić, "Split ratio optimization of high torque density PM BLDC machines considering copper loss density limitation and stator slot leakage," *Int. J. Electr. Power Energy Syst.*, vol. 100, pp. 231–239, Sep. 2018, doi: 10.1016/j.ijepes.2018.02.029.

[4] S.-U. Chung, S.-H. Moon, D.-J. Kim, and J.-M. Kim, "Development of a 20-Pole–24-Slot SPMSM With Consequent Pole Rotor for In-Wheel Direct Drive," *IEEE Trans. Ind. Electron.*, vol. 63, no. 1, pp. 302–309, Jan. 2016, doi: 10.1109/tie.2015.2472375.

[5] M. E. Beniakar, A. G. Sarigiannidis, P. E. Kakosimos, and A. G. Kladas, "Multiobjective Evolutionary Optimization of a Surface Mounted PM Actuator With Fractional Slot Winding for Aerospace Applications," *IEEE Trans. Magn.*, vol. 50, no. 2, pp. 665–668, Feb. 2014, doi: 10/f5t2x8.

[6] M. E. Beniakar, P. E. Kakosimos, and A. G. Kladas, "Strength Pareto Evolutionary Optimization of an In-Wheel PM Motor With Unequal Teeth for Electric Traction," *IEEE Trans. Magn.*, vol. 51, no. 3, pp. 1–4, Mar. 2015, doi: 10/gpc9h2.

[7] Z. Li, X. Huang, Z. Chen, T. Shi, and Y. Yan, "Nonlinear Analytical Analysis of External Rotor Permanent-Magnet Synchronous Motor," *IEEE Trans. Magn.*, pp. 1–1, 2021, doi: 10/gjwdk4.

[8] M. G. Angle, J. H. Lang, J. L. Kirtley, S. Kim, and D. Otten, "Modeling of Surface Permanent Magnet Motors With Cogging and Saturation Effects Included," *IEEE Trans. Energy Convers.*, vol. 33, no. 4, pp. 1604–1613, Dec. 2018, doi: 10.1109/tec.2018.2849926.

[9] M. Shen, P.-D. Pfister, C. Tang, and Y. Fang, "A Hybrid Model of Permanent-Magnet Machines Combining Fourier Analytical Model With Finite Element Method, Taking Magnetic Saturation Into Account," *IEEE Trans. Magn.*, vol. 57, no. 2, pp. 1–5, Feb. 2021, doi: 10.1109/TMAG.2020.3005802.

[10] L. J. Wu, Z. Li, X. Huang, Y. Zhong, Y. Fang, and Z. Q. Zhu, "A Hybrid Field Model for Open-Circuit Field Prediction in Surface-Mounted PM Machines Considering Saturation," *IEEE Trans. Magn.*, vol. 54, no. 6, pp. 1–12, Jun. 2018, doi: 10/gdn68j.

[11] J. Pyrhonen, T. Jokinen, and V. Hrabovcová, *Design of rotating electrical machines*. Chichester, West Sussex, United Kingdom ; Hoboken, NJ: Wiley, 2008.

[12] Z. Q. Zhu and D. Howe, "Instantaneous magnetic field distribution in permanent magnet brushless DC motors. IV. Magnetic field on load," *IEEE Trans. Magn.*, vol. 29, no. 1, pp. 152–158, Jan. 1993, doi: 10/bx2r37.

[13] Z. Q. Zhu, L. J. Wu, and Z. P. Xia, "An Accurate Subdomain Model for Magnetic Field Computation in Slotted Surface-Mounted Permanent-Magnet Machines," *IEEE Trans. Magn.*, vol. 46, no. 4, pp. 1100–1115, Apr. 2010, doi: 10.1109/TMAG.2009.2038153.

[14] T. Reichert, T. Nussbaumer, and J. W. Kolar, "Split Ratio Optimization for High-Torque PM Motors Considering Global and Local Thermal Limitations," *IEEE Trans. Energy Convers.*, vol. 28, no. 3, pp. 493–501, Sep. 2013, doi: 10.1109/tec.2013.2259169.

[15] S. Zhang, W. Zhang, J. Zhao, and R. Wang, "Multi-Objective Optimization Design and Analysis of Double-Layer Winding Halbach Fault-Tolerant Motor," *IEEE Access*, vol. 9, pp. 3725–3734, 2021, doi: 10.1109/ACCESS.2020.3047860.

[16] S. L. Ho, S. Yang, H. C. Wong, K. W. E. Cheng, and G. Ni, "An improved ant colony optimization algorithm and its application to electromagnetic devices designs," *IEEE Trans. Magn.*, vol. 41, no. 5, pp. 1764–1767, May 2005, doi: 10.1109/TMAG.2005.845998.

[17] EvangelosM. Tsampouris, P. E. Kakosimos, and AntoniosG. Kladas, "Coupled Computation of Electric Motor Design and Control Parameters Based on Ant Colonies Speed Trajectory Optimization," *IEEE Trans. Magn.*, vol. 49, no. 5, pp. 2177–2180, May 2013, doi: 10.1109/TMAG.2013.2243909.

[18] J. L. Viegas, S. M. Vieira, and J. M. C. Sousa, "Fuzzy clustering and prediction of electricity demand based on household characteristics," presented at the 2015 Conference of the International Fuzzy Systems Association and the European Society for Fuzzy Logic and Technology (IFSA-EUSFLAT-15), Atlantis Press, Jun. 2015, pp. 1040–1046. doi: 10.2991/ifsa-eusflat-15.2015.147.

[19] M. Versaci, G. Angiulli, P. Crucitti, D. De Carlo, F. Laganà, *et al.*, "A Fuzzy Similarity-Based Approach to Classify Numerically Simulated and Experimentally Detected Carbon Fiber-Reinforced Polymer Plate Defects," *Sensors*, vol. 22, no. 11, p. 4232, Jun. 2022, doi: 10.3390/s22114232.